Current-Voltage Relations of the Apical and Basolateral Membranes of the Frog Skin

HOWARD F. SCHOEN and DAVID ERLIJ

From the Department of Physiology, Downstate Medical Center, State University of New York, Brooklyn, New York 11203

ABSTRACT We determined the current-voltage (*I-V*) relations of the apical and basolateral barriers of frog skins by impaling the cells with an intracellular microelectrode and assuming that the current across the cellular pathway was equal to the amiloride-inhibitable current. We found that: (*a*) The responses in transepithelial current and intracellular potential to square pulses of transepithelial potential (V_T) varied markedly with time. (*b*) As a consequence of these transient responses, the basolateral *I-V* relation was markedly dependent on the time of sampling after the beginning of each pulse. The apical *I-V* plot was much less sensitive to the time of sampling within the pulse. (*c*) The *I-V* data for the apical barrier approximated the *I-V* relations calculated from the Goldman constant field equation over a relatively wide range of membrane potentials (±100 mV). (*d*) A sudden reduction in apical bath [Na^+] resulted in an increase in apical permeability and a shift in the apical barrier zero-current potential (E_a) toward less positive values. The shift in E_a was equivalent to a change of 45 mV for a 10-fold change in apical [Na^+]. (*e*) The transient responses of the skin to square V_T pulses were described by the sum of two exponentials with time constants of 114 and 1,563 ms, which are compatible with the time constants that would be produced by an RC circuit with capacitances of 65 and 1,718 μF. The larger capacitance is too large to identify it comfortably with a true dielectric membrane capacitance.

INTRODUCTION

Recently, much interest has been devoted to the analysis of the current-voltage (*I-V*) relations in tight epithelia (Fuchs et al., 1977; Helman and Fisher, 1977; Frömter et al., 1981; Thompson et al., 1982*a*, *b*). It has been hoped that such an analysis would provide insights into the fundamental mechanisms of ion transport as well as the mode of action of modifiers. In this communication, we describe experiments in which we used a microelectrode to determine the *I-V* relations of both the apical and basolateral membranes of the frog skin.

Address reprint requests to Dr. Howard F. Schoen, Dept. of Physiology, 31, Downstate Medical Center, State University of New York, 450 Clarkson Ave., Brooklyn, NY 11203.

J. GEN. PHYSIOL. © The Rockefeller University Press · 0022-1295/85/08/31/0257$1.00

Volume 86 August 1985 257–287

Previous measurements of *I-V* relations in the frog skin have been based on two radically different approaches (Fuchs et al., 1977; Helman and Fisher, 1977). On the one hand, Fuchs and co-workers made transepithelial measurements in skins bathed with solutions of high K^+ concentration on the serosal side. These authors claimed that a high serosal K^+ concentration reduces the basolateral membrane's resistance and potential to levels low enough to virtually eliminate the contribution of this membrane to the electrical measurements. To differentiate between cellular and paracellular currents, these authors assumed that the amiloride-sensitive current represents the cellular current. Their measurements of amiloride-sensitive currents were well fitted by the Goldman equation in a range of 0–50 or 0–100 mV.

On the other hand, Helman and Fisher (1977) have used microelectrodes to distinguish the apical and basolateral membranes. However, they interpreted their data on the basis of the following assumptions. (*a*) The transepithelial *I-V* relation is made up of several linear regions that are separated by well-defined "breaks" (Helman and Miller, 1971). (*b*) One of these breaks in the linearity of the *I-V* plot (which they designate E_1) corresponds to the point where V_T (the transepithelial potential) equals E_{Na}, the electromotive force of the transepithelial transport system (Helman et al., 1975). (*c*) From this it follows that when the skin is brought to the potential equal to E_1, no current passes through the cell pathway for Na^+ transport, i.e., all the current flowing in such a condition is moving along shunt pathways. Hence, determination of E_1 allows the calculation of the shunt conductance. (*d*) The shunt conductance calculated at E_1 is constant over a wide range of potentials and one can therefore use it to calculate the cell currents by subtracting the estimated shunt current from the total transepithelial currents. The cell currents thus calculated can be used to produce an *I-V* plot of the transport pathway. (*e*) More recently, Helman and Fisher (1977) and Helman et al. (1979) have concluded that when the skin is brought to the potential equal to E_1, the apical membrane potential is zero, and that one can therefore determine E_{Na} by observing what value of transepithelial potential will bring the apical potential to zero.

Our approach has been to study the individual membranes using microelectrode techniques, and to differentiate between cellular and paracellular currents as did Fuchs et al. (1977), namely, by assuming that the cell membrane current (I_m) is equal to the amiloride-inhibitable current.

At the onset of our experiments, we discovered that sudden changes of V_T were followed by transient changes in I_m and V_a. Therefore, we also examined the influence of this transient behavior on the interpretation of our results.

Some of these data have been published in preliminary form (Schoen and Erlij, 1981*a*, *b*, 1982).

LIST OF SYMBOLS

I_T	total transepithelial current
I_{sc}	short-circuit current; I_T when $V_T = 0$
I_{am}	I_T in the presence of amiloride
I_m	membrane or transcellular current (positive when flowing from inside to outside the cell); $I_T - I_{am}$ (transcellular or basolateral) or $I_{am} - I_T$ (apical)

I_m^{sc} I_m when $V_T = 0$
V_T transepithelial voltage (serosal bath = 0)
V_a apical membrane voltage (apical bath = 0)
V_a^{sc} V_a when $V_T = 0$
V_b basolateral membrane voltage (serosal bath = 0); $V_a + V_T$
g_T total transepithelial conductance; $\Delta I_T/\Delta V_T$, estimated from data obtained when $V_T = +20$ and -20 mV or 0 and -40 mV
g_a slope conductance of apical membrane; $\Delta I_m/\Delta V_a$, estimated from data obtained when $V_T = +20$ and -20 mV or 0 and -40 mV
g_b slope conductance of basolateral membrane; $\Delta I_m/\Delta V_b$, estimated from the same data as g_a
g_P slope conductance of "shunt pathway," estimated as g_T in the presence of amiloride; $\Delta I_{am}/\Delta V_T$ (with $V_T = +20$ and -20 mV)
G_a chord conductance of apical membrane; $I_m^{sc}/(V_a^{sc} - E_a)$
G_b chord conductance of basolateral membrane; $I_m^{sc}/(V_a^{sc} - E_b)$
E_a zero-current potential, or emf, of apical barrier; V_a when $I_m = 0$
E_b zero-current potential, or emf, of basolateral barrier; V_b when $I_m = 0$
E_{Na} total zero-current potential, or emf, for transepithelial Na^+ transport; V_T when $I_m = 0$
f fractional resistance of the apical barrier; measured as $-\Delta V_a/\Delta V_T$ (with $V_T = 0$ and -40 mV)
f' fractional resistance of the apical barrier; calculated as $(1/g_a)/(1/g_a + 1/g_b) = g_b/(g_a + g_b)$

METHODS

Conventions

Transepithelial current (I_T) is expressed such that inward current (that is, current flowing from the apical, or mucosal, side to the basolateral, or serosal, side) is considered positive. Transepithelial voltage (V_T) is expressed with the serosal bath as zero. Hence, the short-circuit current is positive and the open-circuit potential is negative (see Fig. 4 for an example).

A separate set of conventions is used for describing the currents and voltages across individual cell membranes, namely, the conventions commonly used by cell electrophysiologists in describing the electrical properties of single cells or nerve fibers. Transmembrane currents flowing into the cell are taken as negative regardless of whether the apical or basolateral membrane is being considered. Note that, according to this convention, when the skin is short-circuited, the apical membrane current is negative, whereas the basolateral membrane current is positive, since current flows into the cell across the apical membrane but exits across the basolateral membrane. Membrane voltage is expressed relative to the bathing solution in contact with the particular membrane being described. With this convention and the convention for V_T, the basolateral membrane voltage is calculated from the relation

$$V_b = V_a + V_T. \quad (1)$$

Animals

Frogs were either bullfrogs, *Rana catesbeiana*, from the Dominican Republic, or grass frogs, *R. pipiens*, obtained from Connecticut Valley Biological Supply Co., Southampton, MA. Animals were killed by double pithing. The abdominal skin was dissected off and a

circular piece was mounted in a horizontal Ussing-type chamber (Helman and Fisher, 1977). In early experiments, the skin was simply clamped between the two half-chambers. In later experiments, to reduce edge leakage, the upper half of the chamber was fixed in place by gluing it (Helman and Miller, 1971) to the apical side of the skin with a cyanoacrylic-type adhesive (Histoacryl, B. Braun Melsungen, Melsungen, Federal Republic of Germany). The skin was supported underneath by a 150-mesh stainless steel screen (Small Parts, Inc., Miami, FL). The lower chamber was kept at a negative pressure of 30–60 cm H_2O.

The current and voltage electrodes were Hg/Hg_2Cl_2-saturated KCl half-cells and were connected to the chamber by 3 M KCl/agar bridges. The upper bath was grounded via an Ag/AgCl electrode inserted into a 3 M KCl/agar bridge.

Criteria for Successful Impalements

Intracellular potentials were measured with standard open-tipped microelectrodes (6–12 MΩ) made from fiber-filled 1-mm capillaries (W-P Instruments, Inc., New Haven, CT, or Frederick Haer & Co., Brunswick, ME) and filled with 3 M KCl. Impalements were accepted only if (*a*) the electrode resistance was not more than 25 MΩ higher inside the cell than outside, (*b*) the intracellular potential was stable within ±2 mV for at least 10 min and was no more than 10 mV from the initial value on impalement, and (*c*) the addition of amiloride caused an increase in the negativity of the intracellular potential and an increase in the apical membrane fractional resistance (f) to at least a value of 0.95. Furthermore, shortly after impaling a cell, the quality of the impalement was checked by ascertaining that slight vertical movements of the microelectrode both up and down did not alter V_a^{sc} or electrode resistance.

Experimental Procedure

The general features of our procedure are shown in Fig. 1. The skin was continuously maintained at short circuit ($V_T = 0$), except for brief intervals (600 ms every 20 s) when V_T was changed to −40 mV in order to monitor transepithelial conductance and f. The V_T change was accomplished by having a microcomputer change the command voltage to a voltage clamp. To measure the *I-V* relations, V_T was changed periodically to a series of nonzero values. Although several protocols were used, the most common series of pulses was that shown here, namely, the sequence V_T = 20, −20, 40, −40, 60, −60, 80, −80, 100, −100, 120, −120, 140, −140, −160, −180, and −200 mV. A timer module in the computer measured the time from the start of each pulse. The computer was programmed to sample the parameters from the experimental apparatus at several specific times after the pulse began. This allowed us to plot *I-V* data obtained for many different time delays from a single series of pulses. After each pulse, the computer returned the command voltage to zero, thereby returning the skin to short circuit. The skin was then held at short circuit for a period of at least 15 times the length of the pulse period before another pulse was given. After the series, 100, or, as in this case, 20 μM amiloride was added to the apical bath. After 1–2 min, a second series of pulses was sent to obtain I_{am}.

For the data analysis, I_T obtained in the presence of amiloride (I_{am}) at each V_T was subtracted from the I_T values obtained in the absence of amiloride to obtain the net cellular current, I_m, according to the relation

$$I_m = I_T - I_{am}. \tag{2}$$

In experiments in which two apical bath Na^+ concentrations were compared, two series of pulses in the presence of amiloride were obtained, one at each Na^+ concentration.

In some experiments, the time course of the response to pulses of $V_T = 20$ or -20 mV of several seconds' duration were measured. These data were analyzed by the BMDP3R program (October 1983 revision) of the Biomedical Computer Programs developed at the Health Sciences Computing Facility, University of California, Los Angeles, CA (Dixon, 1983).

Instrumentation

In our early experiments, a voltage-clamp/microelectrode amplifier system, virtually identical to that described by Helman and Fisher (1977), was used. V_a and I_T were recorded on digital panel meters or on a model 1200 two-channel chart recorder (MFE Corp., Salem, NH) for later analysis. Later, the circuit was modified by the substitution

FIGURE 1. Tracings illustrating the general procedure involved in determining the *I-V* relations. The upper tracing is the intracellular potential; the lower tracing is the transepithelial current. Initially, the skin was held at short circuit, except that pulses of 600 ms duration and -40 mV were passed every 20 s. Then, to determine the control *I-V* relation, a series of pulses of continuously increasing amplitude was passed in both the hyperpolarizing and the depolarizing direction. At the left arrow, amiloride (20 μM) was added to the apical-side solution. The characteristic increase in intracellular potential and inhibition of I_{sc} was produced. Then, another series of pulses was passed. Finally, the amiloride was washed out (right arrow).

of a M-707 microprobe system (W-P Instruments, Inc.) for the microelectrode amplifier (see Fig. 2). Also, a capacitor (0.001 μF) and variable resistor (1 MΩ) in series (not shown) were placed in the feedback loop of amplifier A_2. The adjustment of this resistor permitted the optimization of the response speed of the clamp. A response time of 1 ms was usually attainable. No correction was made for solution resistance. The whole apparatus was coupled to an S-100 bus microcomputer (Tecmar, Inc., Cleveland, OH) for control of V_T and for the recording of V_a and I_T (see below).

The central processing unit of the computer was an eight-bit Z-80A microprocessor (Mostek Corp., Carrollton, TX). The computer was coupled to floppy disks for storage of data. It also was equipped with an S-100 digital-to-analog converter board and an analog-to-digital converter board with a 16-channel multiplexer. The microcomputer could send, via the digital-to-analog converter, a command voltage to the voltage clamp

for the control of V_T. The analog-to-digital converter was used for the recording of V_T, V_a, and I_T. In this way, we were able to collect data automatically at multiple points in time after the beginning of an alteration in V_T. The electrical parameters were also routinely monitored on the chart recorder and on a storage oscilloscope (model 5111, Tektronix, Inc., Beaverton, OR). Data were analyzed and plotted on a DMP-7 plotter (Houston Instruments, Austin, TX) driven by the computer via a standard RS-232

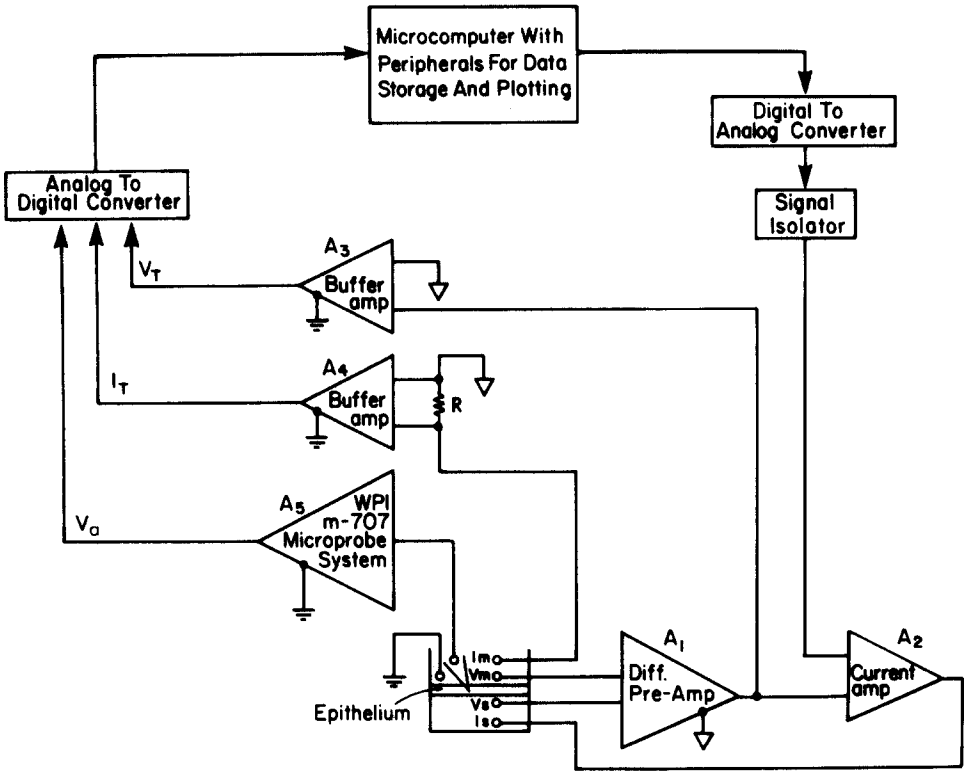

FIGURE 2. Scheme of the recording and voltage-clamping arrangement used in these experiments. Amplifiers A_1 and A_2 constitute the voltage-clamp circuit and use a ground-isolated power supply with a floating reference (open arrow). Input to the voltage clamp from the microcomputer, via the digital-to-analog converter, signal isolator, and A_2, controls the transepithelial potential (V_T). Current flowing through the tissue is measured by the voltage drop across resistor R. This voltage is then buffered by A_4. The intracellular potential monitored by the microelectrode is amplified by A_5. The signals from A_3, A_4, and A_5 are converted under computer control to digital signals by the analog-to-digital converter and then stored by the computer on a floppy disk for subsequent analysis.

interface. The software for the data acquisition and analysis was written in a mixture of Forth and Z-80 assembly language.

The correct grounding and referencing of signals is important for the minimization of noise. To this end, the voltage amplifier (A_1) and the current amplifier (A_2) of the voltage clamp were referenced to the ground-isolated common of their bipolar battery power supply. The chamber solution was connected to this reference via one of the current

electrodes. The microelectrode amplifier (A_3) was referenced to the upper bath earth-ground electrode. To allow a faster settling time for the analog-to-digital converter, the floating signals from A_1 and across the current-sensing resistor R were converted into ground-referenced signals by amplifiers A_3 and A_4 (FET-input instrumentation amplifier, model 3621, Burr-Brown Research Corp., Tucson, AZ), respectively, before sending them to the analog-to-digital converter.

The digital-to-analog converter signal to the voltage clamp was isolated by a model SIU5 stimulus isolation unit (Grass Instrument Co., Quincy, MA). Because this unit produces an output of only a single polarity, the signal was converted to a bipolar one by the addition to the circuit of a separate, ground-isolated, constant-voltage signal (not shown). The constant voltage was then coupled, via an adder circuit, with the signal from the isolator and sent to amplifier A_2.

Solutions

Cl^- Ringer's (Hodgkin and Horowicz, 1959) contained (mM): 115 NaCl, 2.5 KCl (or 5.0 where noted), 1.8 $CaCl_2$, 2.16 Na_2HPO_4, and 0.86 NaH_2PO_4. Low-Na^+ Ringer's was identical to the Cl^- Ringer's except that Na^+ was substituted for with choline or tetraethylammonium. An activity coefficient for univalent ions of 0.76 was calculated for these solutions from the Davies approximation of the Debye-Hückel equation (Robinson and Stokes, 1965).

SO_4^{2-} Ringer's contained (mM): 56 Na_2SO_4, 1.25 K_2SO_4, 2.4 $NaHCO_3$, and 8 $CaSO_4$. The calculated activity coefficient was 0.73.

Amiloride was a gift of Merck, Sharp & Dohme (West Point, PA) and was used at 20 or 100 μM.

RESULTS

Transient Responses to Square V_T Pulses

Fig. 3*A* illustrates the responses of transepithelial voltage (V_T), apical membrane voltage (V_a), and the transepithelial current (I_T) when the command voltage was changed from 0 to −40 mV. Even though the change in V_T was complete after a very short delay (1–2 ms), V_a and I_T were still changing after 600 ms. Fig. 3*B* shows that most of the transient behavior was eliminated after the skin was treated with amiloride. Similar long-lasting responses to step changes of voltage have been observed previously in epithelial tissues (see, for example, Nagel, 1976; Weinstein et al., 1980).

Fig. 4 shows typical plots for I_T vs. V_T. The two control plots shown (symbols connected by solid lines) were obtained from a single series of pulses but with the data sampled at 20 and 600 ms after the initiation of the pulses (see Methods). It is clear that the conductance, as estimated from the slope, and the open-circuit potential difference, as estimated from the *V*-axis intercept, depend on the time of sampling. In this example, the conductance in the vicinity of the short-circuit point was 0.56 mS/cm^2 when calculated from the data sampled at 20 ms, but 0.43 mS/cm^2 when calculated at 600 ms. The apparent open-circuit potential difference increased from −46.5 mV at 20 ms to −58.8 mV at 600 ms. Fig. 4 also shows a plot for I_T vs. V_T for the skin after the addition of amiloride (dotted curve). Amiloride reduced the conductance (to 0.18 mS/cm^2) and the short-circuit current (from 23.8 to 0.5 μA/cm^2). Only a single time of sampling is shown for amiloride, since, as shown in Fig. 3*B*, the amiloride responses varied

only slightly or not at all with time. A summary of all the transepithelial data is given in Table I as calculated from the 600-ms samples.

The vertical displacement between the control and the amiloride curves in Fig. 4 corresponds to $I_T - I_{am}$, which we assume is equal to the net Na^+ (cellular) current (I_m). The point at which each control curve crosses the amiloride curve represents the zero cellular current point. The cellular currents to the right of

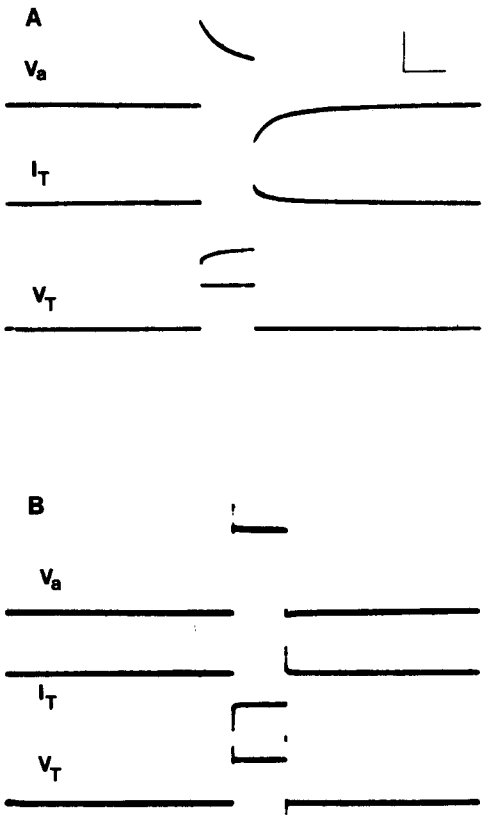

FIGURE 3. Oscilloscope tracings showing the response in intracellular potential (V_a), transepithelial current (I_T), and transepithelial potential (V_T) to a change in the control voltage to the clamp. (The deflections in I are downward.) (*A*) Control records. (*B*) Amiloride-treated skin. Both tracings were recorded while the microelectrode was in the same cell. The vertical scale marker equals 20 mV (V_a), 10 μA (I_T), and 40 mV (V_T); the horizontal scale marker equals 500 ms.

these points are flowing from the mucosal to the serosal bathing solutions, and to the left, from the serosal to the mucosal. Also, at these points, V_T equals the total emf for Na^+ transport across the skin (E_{Na}). Thus, it is clear that the value calculated for E_{Na} also depends on the time chosen for analysis.

In Fig. 5, we have plotted the net cellular current (I_m) against V_T. The values of I_{am} used to calculate I_m in this and in all subsequent figures and calculations

were sampled with the same delay after the beginning of the pulse as the corresponding I_T, despite the virtual lack of transients in the amiloride-treated tissues. The slope of this curve represents the transcellular conductance, and the V intercept represents the zero cellular current point. This figure shows again that, in general, as the data are sampled later in the pulse, the apparent value of E_{Na} becomes higher. In this example, E_{Na} rose from −69.2 mV at 20 ms to −92.7 mV at 600 ms. The calculated cellular slope conductance also fell when the sampling delay was longer. In this experiment, it dropped from 0.38 mS/cm^2 at 20 ms to 0.24 mS/cm^2 at 600 ms.

Evidently, a valid analysis of the *I-V* relations of the barriers of the skin cannot be made without assessing the effect of sampling time on the shape of the *I-V* plots. Hence, in the following sections, particular attention will be focused on describing the influence of sampling time on the interpretation of electrical measurements.

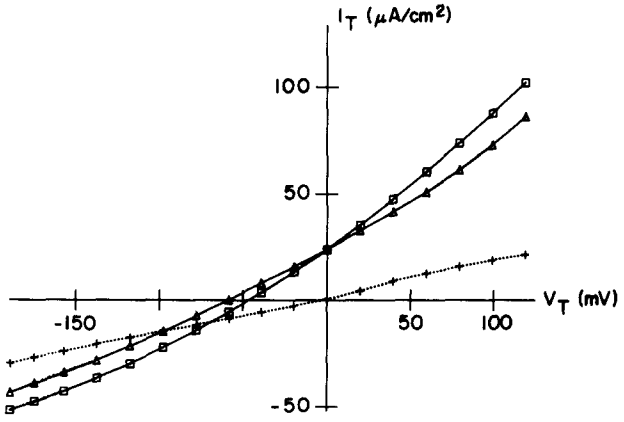

FIGURE 4. Plots of transepithelial current (I_T) as a function of transepithelial voltage (V_T). Solid lines, control; dotted line, plusses, amiloride. Two values of I_T determined at two different times during each voltage pulse are plotted for the control curve: □, 20 ms; △, 600 ms.

Apical Border

With the values of I_m obtained as described above, together with the measurement of V_a obtained with the microelectrode, it was possible to analyze the *I-V* relations of the individual transport barriers. Examples of results obtained for the apical membrane, with I_m plotted against V_a, are shown in Figs. 6 and 7 for experiments done in either Cl^- or Cl^--free (SO_4^{2-}) solutions, respectively. Each panel shows *I-V* data sampled at several different times during the same series of V_T pulses.

Except as noted below, all the points, regardless of the sampling time, tend to fall along the same curve. This behavior arises because both V_a and I_m tend to change in concert. Because of the similarity in the curves for data collected at different times, it is not surprising that, in general, there was little effect of time of measurement on the values calculated for the apical membrane parameters in

Figs. 8 and 9. In these figures, the calculated values of g_a (Fig. 8) and E_a (Fig. 9) for each skin have been plotted against the time delay used for the collection of the raw data.

E_a (Fig. 9) appeared to vary with time somewhat more than g_a (Fig. 8). This is not surprising, because E_a is estimated as the V_a intercept; small errors in the estimation of I_m, in particular, can have a relatively large effect on the position

TABLE I

*Summary of Parameters of the Apical and Basolateral Membranes**

	R. pipiens		*R. catesbeiana*	
Ringer's	Cl^-	SO_4^{2-}	Cl^-‡	SO_4^{2-}
n	1	2	9	5
I_{sc}	23.8	32.5±4.2	34.1±8.3	17.5±6.3
V_{oc}	−58.8	−61.8±13.9	−49.7±9.2	−89.1±12.1
g_T	0.43	0.62±0.19	0.74±0.16	0.33±0.08
V_a^{sc}	−40.5	−32.6±2.9	−51.8±3.4	−37.5±3.1
E_a	21.3	28.9±3.2	49.7±5.4	53.4±6.2
E_b	−75.9	−82.0±1.6	−94.4±2.3§	−76.1±7.2
E_{Na}	−97.2	−110.9±4.8	−144.1±5.3	−131.8±8.6
I_{sc}^{am}	0.5	2.4±1.5	2.9±0.8	3.3±0.4
V_{oc}^{am}	−3.0	−9.6±0.1	−7.5±1.3	−44.4±6.2
g_p	0.18	0.24±0.15	0.48±0.13	0.08±0.01
V_a^{am}	−110.2	−93.9±0.3	−105.4±4.7	−84.9±6.5
g_a	0.44	0.61±0.05	0.41±0.10	0.26±0.10
g_b	0.54	0.75±0.07	0.83±0.28	0.43±0.13
f'	0.55	0.55±0.002	0.62±0.04	0.64±0.06
G_a	0.39	0.53±0.07	0.33±0.08	0.19±0.07
G_b	0.67	0.67±0.15	0.89±0.26	0.40±0.10
a_{Na}^s‖	39.7	27.3±3.3	15.8±3.7	11.7±3.0
P_{Na}¶	14.3	32.3±1.5	14.6±3.4	14.4±5.6

* I (μA/cm²); V and E (mV); g and G (mS/cm²); P_{Na} (nm/s); a_{Na}^s (mM). g and G are the slope and chord conductances, respectively, calculated as described in the List of Symbols. V_{oc} is the open-circuit potential interpolated from the I_T vs. V_T plot; V_{oc}^{am} is V_{oc} after amiloride; I_{sc}^{am} is I_{sc} after amiloride; and V_a^{am} is V_a^{sc} after amiloride (peak value). Other symbols are defined in the List of Symbols or in the text. Parameters for the apical membrane are generally from the 20-ms samples; transepithelial parameters and parameters for the basolateral membrane are generally from the 600-ms samples. Means ± standard error.

‡ Includes four skins with 5 mM K^+ in the bathing solution.

§ Two skins with no V_b intercept at 400 ms or later have been omitted.

‖ Calculated from E_a for each skin according to Eq. 4.

¶ Calculated from a_{Na}^a, a_{Na}^s, V_a^{sc}, and I_m^{sc} for each skin according to Eq. 3.

of this intercept. Most of these variations seem to have no consistent relation to time, and the range of variation usually did not exceed ~10 mV.

Although, as generally asserted above, the shape of the I_m vs. V_a curves was little affected by sampling time, there are several deviations that have to be noted. The most frequent deviation in SO_4^{2-} Ringer's is easily seen in Fig. 7. In the hyperpolarizing region of the curve, the points sampled at times longer than 40 ms tend to form a curve that is different from that formed by the values sampled earlier in the pulse. There is also a second deviation, which, although

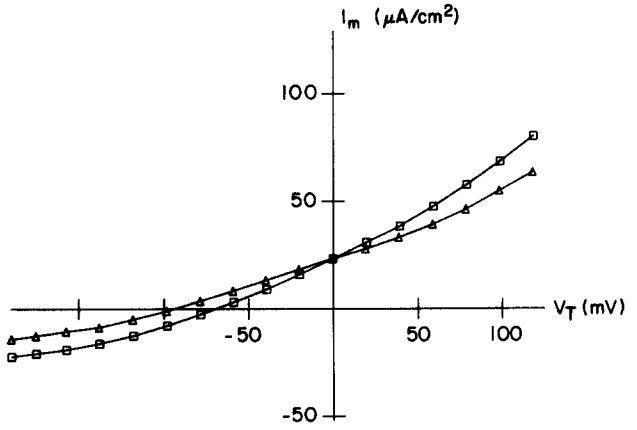

FIGURE 5. Plots of the transcellular current (I_m) as a function of V_T for the skin shown in Fig. 4. The values of I_m were calculated by subtracting the current recorded in the presence of amiloride from the total current before amiloride was added. □, 20 ms; Δ, 600 ms.

slight, appears consistently in SO_4^{2-} Ringer's. This is seen in Fig. 7*B*. Between the transepithelial short-circuit point and the reversal potential, the points sampled at 600 ms and longer lie slightly above the curve traced by the earlier points.

The effect of these two types of deviation is a small, gradual increase in the calculated value of g_a with time. This can be seen in Fig. 8*B*. Note that g_a does not tend to increase with time in Cl^- Ringer's (Fig. 8*B*). This is consistent with

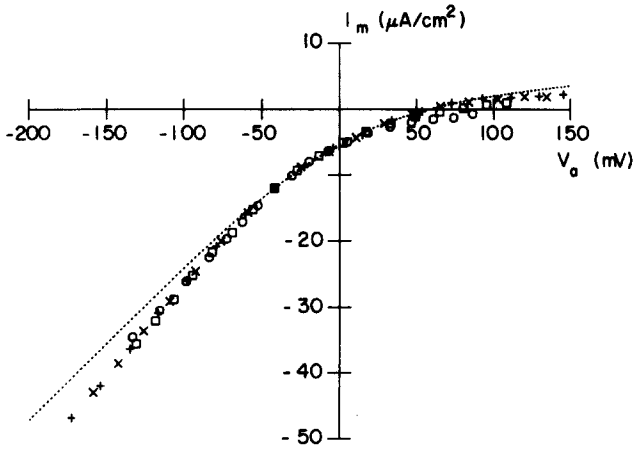

FIGURE 6. *I-V* relation of the amiloride-inhibitable pathway of the apical border of a skin from *R. catesbeiana* in Cl^- Ringer's. Membrane current (I_m) and apical membrane potential (V_a) were determined at several times during each pulse. Each individual sampling time is identified by the indicated symbol. The dotted curve was drawn as described in the text. +, 20 ms; ×, 60 ms; □, 200 ms; O, 600 ms.

the absence of these deviations in Cl^- Ringer's. A third type of deviation was seen on some occasions in both SO_4^{2-} and Cl^- Ringer's. This can be seen in Fig. 6 for a skin incubated in Cl^- Ringer's and in Fig. 7*B* for SO_4^{2-} Ringer's and occurs at large positive values of V_a. In this region, the points sampled after 20 ms have a tendency to form separate curves for each sampling time. This deviation often resulted in progressively higher values for the voltage intercept

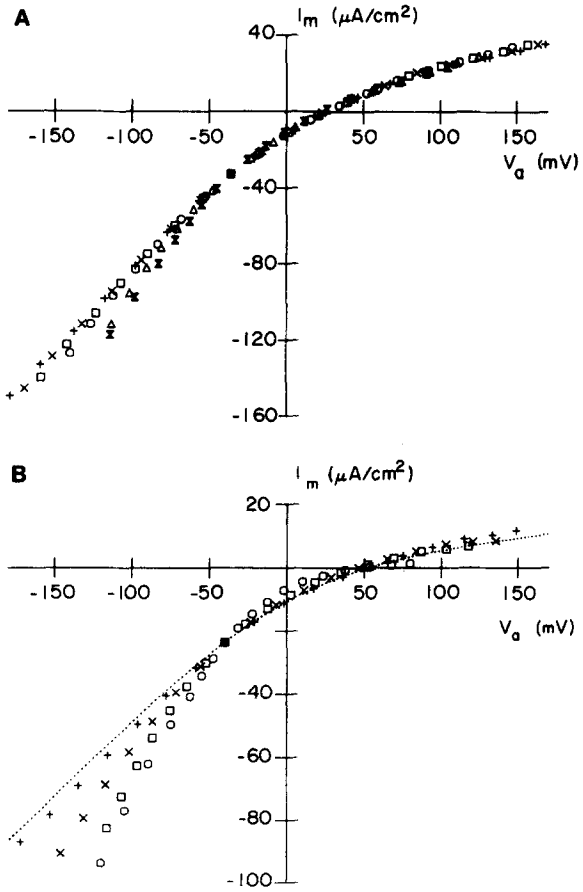

FIGURE 7. *I-V* relation of the amiloride-inhibitable pathway of the apical border of the skin in SO_4^{2-} Ringer's, drawn as described for Fig. 6. *A* is from an experiment carried out on *R. pipiens*; *B* is from an experiment on *R. catesbeiana*. (*A*) +, 4 ms; ×, 10 ms; □, 20 ms; ○, 40 ms; △, 100 ms; ⧗, 200 ms. (*B*) +, 4 ms; ×, 40 ms; □, 100 ms; ○, 600 ms.

(E_a) when working in Cl^- solutions but not in the SO_4^{2-} experiments (compare also Fig. 9, *A* and *B*). In the skin shown in Fig. 6, the curve determined with the longest sampling time had no *V* intercept. Similar behavior was observed in two other skins in Cl^- Ringer's.

A summary of all results obtained for the apical border is included in Table I. The calculated results for this barrier are all from the 20-ms data, except for a

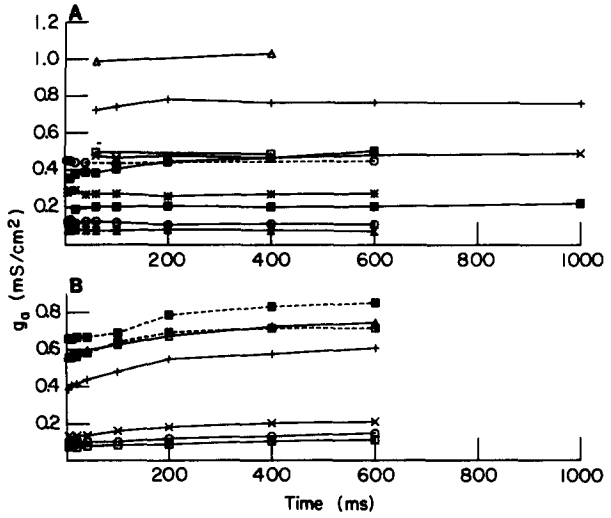

FIGURE 8. Plot of g_a (the calculated slope conductance of the apical membrane near $V_T = 0$) as a function of sampling time. (*A*) Experiments in Cl^- Ringer's. (*B*) Experiments in SO_4^{2-} Ringer's. In Figs. 8, 9, 12, and 13, each symbol type represents a single experiment. The symbols connected by the solid lines represent *R. catesbeiana*, and those by broken lines, *R. pipiens*.

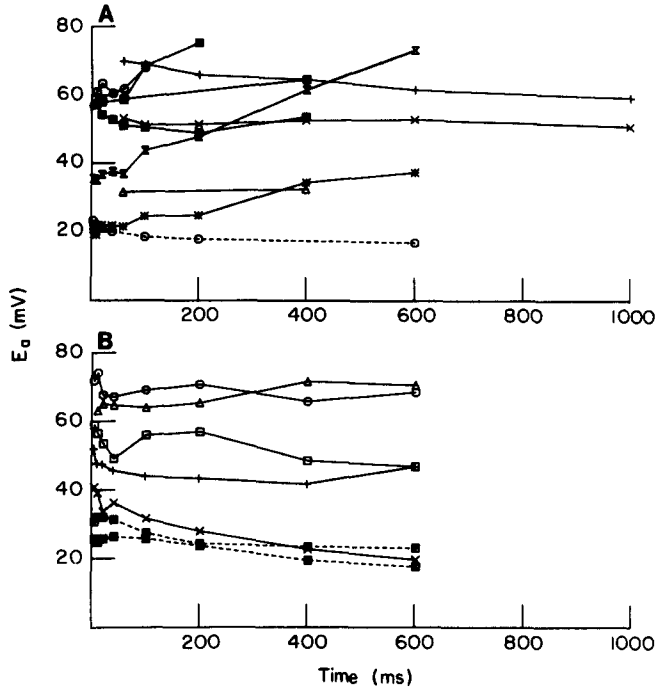

FIGURE 9. Plot of E_a (the reversal potential of the apical membrane) as a function of sampling time. (*A*) Experiments in Cl^- Ringer's. (*B*) Experiments in SO_4^{2-} Ringer's. Symbols represent the same experiments as in Fig. 8.

few cases, where the 20-ms data were not available and the 60-ms data were used. a^c_{Na} (intracellular Na^+ activity) and P_{Na} (apical membrane Na^+ permeability) were calculated using Eqs. 3 and 4 as described below.

GOLDMAN CONSTANT FIELD SOLUTION TO THE NERNST-PLANCK FLUX EQUATION The dotted lines shown in Figs. 6 and 7*B* were calculated from the Goldman constant field equation (Goldman, 1943; Hodgkin and Katz, 1949), viz.:

$$I_m = V_a P_{Na} \frac{F^2}{RT} \frac{a^a_{Na} - a^c_{Na} e^{V_a F/RT}}{1 - e^{V_a F/RT}}, \quad (3)$$

where P_{Na} is membrane permeability to Na^+, a^a_{Na} is the Na^+ activity of the apical bath, a^c_{Na} is the Na^+ activity inside the cell, and F, R, and T have their usual thermodynamic meanings. The curves were drawn using the parameters obtained at only two points, the zero cellular current point (from which a^c_{Na} was calculated using Eq. 4 as described below) and the short-circuit ($V_T = 0$) point (which, along with the value for a^c_{Na}, was used to calculate P_{Na}). No attempt was made to fit the curve to all the data points or to any other region of the *I-V* data. The data approximate the drawn curve quite well, particularly at the early sampling times, and in some cases over the extreme membrane voltage range of ±160 mV.

EFFECT OF LOWERED MUCOSAL Na CONCENTRATION If the zero-current potential of the apical border (E_a) represents the Nernst potential for Na^+, then lowering the apical bath Na^+ concentration should cause a lowering of E_a in accordance with the Nernst equilibrium equation:

$$E_a = (RT/F)\ln(a^a_{Na}/a^c_{Na}), \quad (4)$$

provided that the intracellular Na^+ activity does not change.

These experiments were done using very short pulses (20–40 ms). The use of short pulses enabled the skin to return to its steady state much more rapidly after each individual pulse, and hence allowed the use of short intervals between pulses (1–2 s). In addition, the total number of pulses used was reduced. Using this modified protocol, it was possible to complete an *I-V* determination in 12–24 s. Therefore, the *I-V* data collection could be completed within 1 min of altering the Na^+ concentration.

The results of these experiments are presented in Table II. Note that the average change in E_a is equivalent to ~45 mV/decade, i.e., less than the 59 mV/decade predicted by Eq. 4. The discrepancy could be due to a reduction in a^c_{Na} occurring as a consequence of the lowering of a^a_{Na}.

An example of one of these experiments is shown in Fig. 10. The dotted curves are drawn from Eq. 3. Note that even after lowering the apical Na^+ concentration, the data still approximate the predictions of Eq. 3, although not as well for reduced Na^+ concentrations as for the normal concentration in the region to the right of the zero-current potential.

It is also noteworthy that the permeability (P_{Na}) calculated from the Goldman constant field equation was markedly increased by the reduction in the external Na^+ concentration (Table II), even though the skin had been exposed to the low Na^+ for <1 min. The regulation of Na^+ permeability by extracellular Na^+

TABLE II

*Effect of Reduced Apical-side Na^+ Concentration on Apical Membrane emf and Na^+ Permeability, and Intracellular Na^+ Activity**

Apical bath [Na^+]	120 mM	24 mM‡	Change
E_a (mV)	41.8±10.2	11.6±10.1	44.9±2.1 mV/decade
a^c_{Na} (mM)§	25.1±11.2	17.2±7.9	7.9±3.4 mM
P_{Na} (nm/s)‖	5.9±1.4	16.7±3.5	190±9%

* Means ± standard error (n = 5). Four skins were from *R. catesbeiana* and one was from *R. pipiens*.

‡ In two skins, apical bath [Na^+] was 28 mM.

§ Calculated from E_a for each skin according to Eq. 4.

‖ Calculated from a^a_{Na}, a^c_{Na}, V^{sc}_a, and I^{sc}_m for each skin according to Eq. 3.

concentration has been observed previously (Fuchs et al., 1977; Van Driessche and Lindemann, 1979).

Basolateral Border

The potential of the basolateral barrier can be determined from the value of the apical barrier potential and the transepithelial potential, i.e., $V_b = V_a + V_T$ (Eq. 1). As the basolateral border is in series with the apical border, the current through the basolateral barrier is equal to the current through the apical border. The opposite signs of the current at each border are due simply to the use of conventions commonly adopted in cell electrophysiology (see Methods, *Conventions*).

In contrast to the situation at the apical barrier, the *I-V* data for the basolateral barrier show a strong dependence with time of sampling on the resulting plot. An example is shown in Fig. 11. The calculated apparent conductance (i.e., the slope) decreased markedly with time of sampling from the virtually vertical slope of 40.5 mS/cm^2 at 3 ms to 0.42 mS/cm^2 after 600 ms. Similarly, the apparent emf (i.e., the V_b intercept) increased from −41.4 mV, which is near the value of the V_b before the pulse begins (−40.2 mV), to −103.7 mV after 600 ms. As

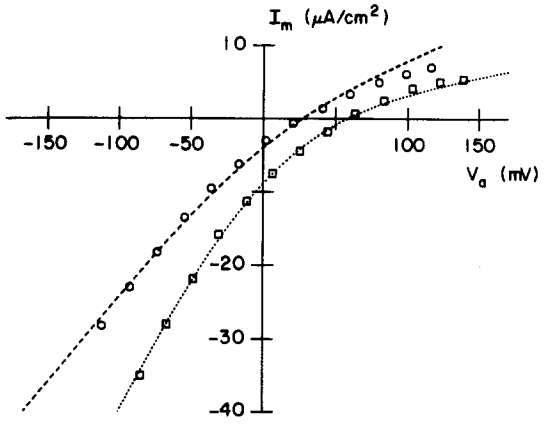

FIGURE 10. Effect of reducing apical Na^+ concentration from 120 (□) to 28 (○) mM (tetraethylammonium substitution) on the *I-V* plot of the apical membrane.

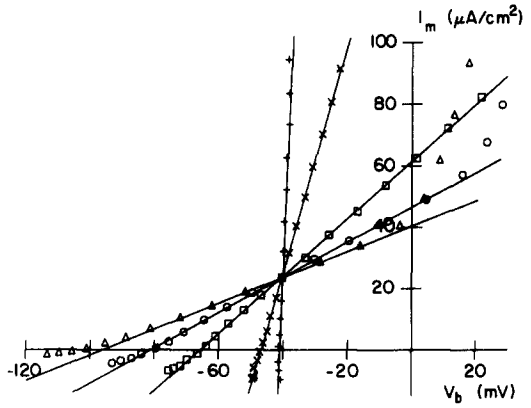

FIGURE 11. *I-V* relation of the amiloride-inhibitable pathway of the basolateral border of the skin. Membrane current (I_m) and basolateral membrane potential (V_b) were determined at several times during each pulse. Each individual sampling time is identified with the indicated symbol: +, 3 ms; ×, 20 ms; □, 100 ms; ○, 200 ms; △, 600 ms.

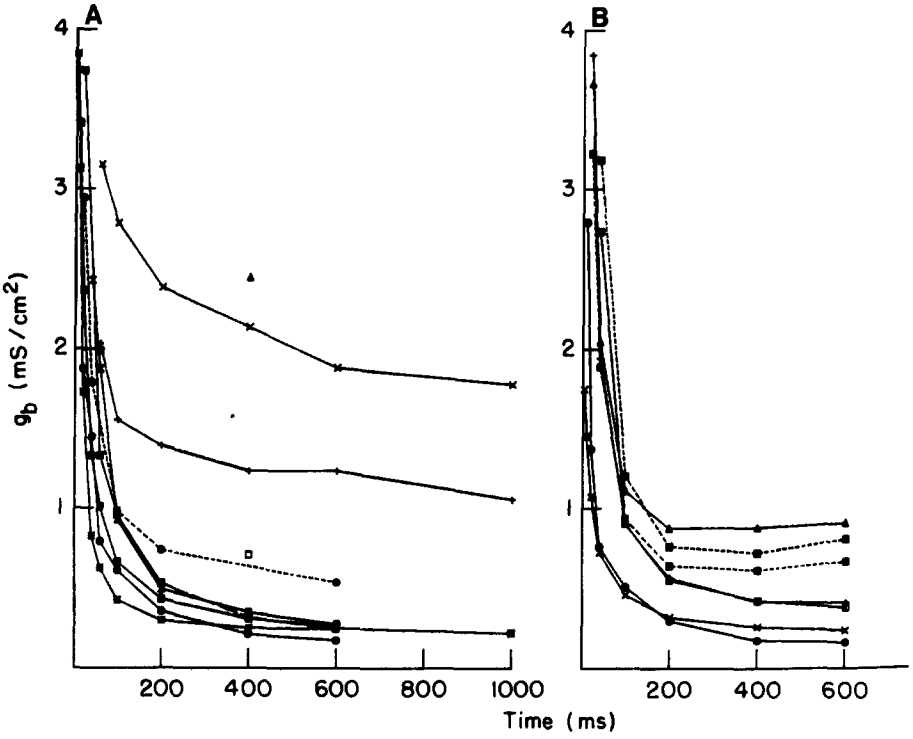

FIGURE 12. Plot of g_b (the calculated slope conductance of the basolateral membrane near $V_T = 0$) as a function of time. (*A*) Experiments in Cl^- Ringer's. (*B*) Experiments in SO_4^{2-} Ringer's. Symbols represent the same experiments as in Fig. 8. Values of conductance >4 mS/cm^2 are omitted. (Only one point is shown for the experiment represented by the triangle in *A*. The only other value obtained for this skin [at 60 ms] was >4 mS/cm^2.)

shown in Figs. 12 and 13, this change in the parameters with time of sampling was a consistent finding for the basolateral barrier.

The *I-V* plots were usually linear, except in the range of the more strongly hyperpolarizing voltages, for times up to 100 ms. This is emphasized by the straight lines drawn in Fig. 11. At 200 ms and later, an additional nonlinearity always appeared around the region where V_b is positive. The *I-V* relationship of the basolateral membrane of the rabbit descending colon has also been reported to have a linear region (from −50 to 0 mV, Wills et al., 1979; from −140 to +110 mV, Thompson et al., 1982*b*).

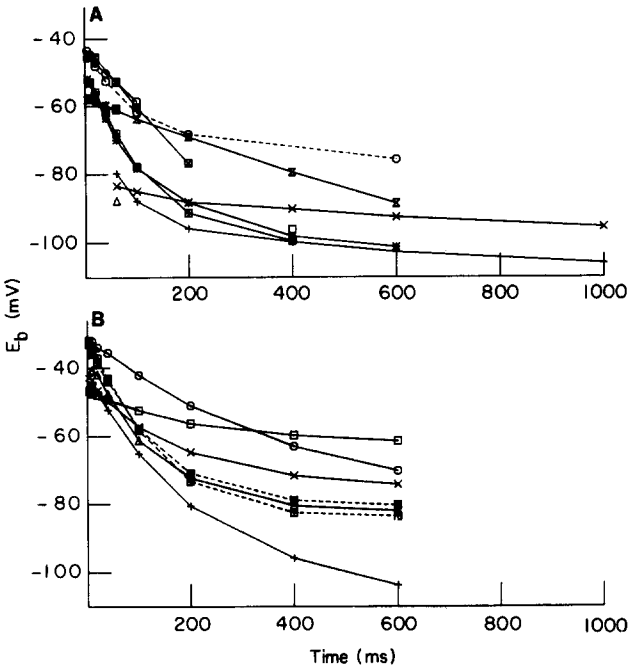

FIGURE 13. Plot of E_b (the reversal potential of the basolateral membrane) as a function of sampling time. (*A*) Experiments in Cl^- Ringer's. (*B*) Experiments in SO_4^{2-} Ringer's. Symbols represent the same experiments as in Fig. 8.

Although it is not shown in Fig. 11, there was no apparent fit of the data at any time to Eq. 3 written for a K^+-selective membrane.

A summary of all results obtained for the basolateral border is included in Table I. The calculated results for this barrier are all from the 600-ms data, except in a few cases where the 600-ms data were not available and the 400-ms data were used. As indicated in Figs. 12 and 13, the calculated parameters have similar values at both times. A justification for the use of the 600-ms data is given in the Discussion.

Kinetic Analysis of the Transient Response

To obtain a more complete description of the time course of the transients, we measured, in three skins incubated in Cl^- Ringer's, the responses to pulses of 3–

8 s duration. To reduce the possibility of permanent changes caused by the long pulses, only small transepithelial voltages were applied (±20 mV).

Fig. 14 is an example of a plot of the magnitude of the transient as a function of time after the beginning the pulse, measured in a single pulse. The ordinate, drawn to a logarithmic scale, is either $I_T - I_T^{inf}$ (upper panel) or $V_a^{inf} - V_a$ (lower

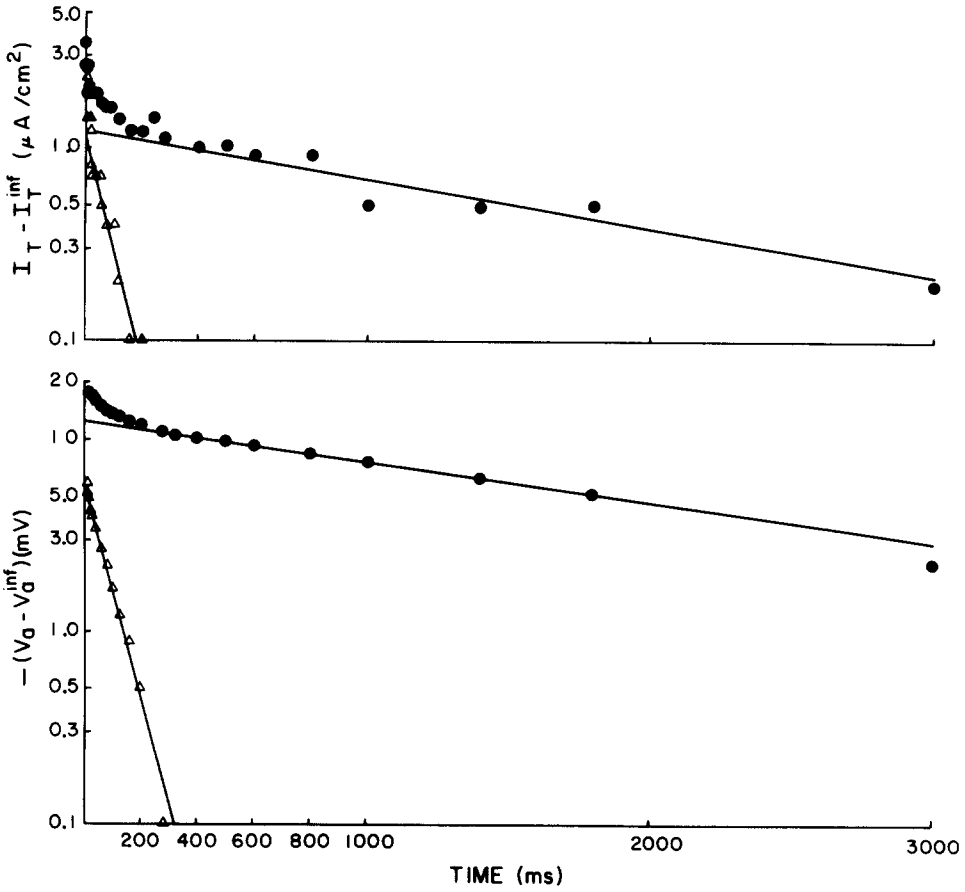

FIGURE 14. Semilogarithmic plots of the value of the amplitude of the transient response in I_T (upper panel) and V_a (lower panel) as a function of time after the initiation of a V_T pulse of 20 mV. The solid symbols represent the data points. The function represented by the line drawn through the solid symbols has a time constant referred to in the text as τ_x. The open symbols represent the value of the data points minus the value of this function. The time constant of the function represented by the line drawn through the open symbols is referred to in the text as τ_b.

panel). I_T^{inf} and V_a^{inf} are I_T and V_a, respectively, determined at the time when there was no further detectable change of I_T and V_a. The straight lines drawn through the linear region of the data (filled circles) were fitted by eye. The functions represented by these lines were then subtracted from the data values and the difference was plotted (open triangles). Straight lines were then fitted

by eye through these points. It thus appeared that the data could be described by the sum of two exponential expressions.

The data were analyzed by a curve-fitting program (see Methods) that provides least-squares estimates of the parameters of a multiexponential function. The results of this analysis gave time constants of 113.6 ± 20.0 and 1,563 ± 322 ms (means ± standard error). Inspection of plots of residuals vs. the dependent variable revealed no evidence of a systematic deviation of observed from predicted values. In some determinations, the analysis showed the presence of an additional exponential component with a time constant of 1–10 ms. Indeed, some indication that an additional component with a shorter time constant might be present can also be seen in Fig. 14, particularly in the upper panel. The time resolution of our measurements was, however, insufficient for a reliable quantitation of this component.

DISCUSSION

The main goal of this study was to provide a reliable description of the *I-V* relations of the individual membranes in the frog skin. Such determinations are important in establishing the mechanism of permeation across the individual barriers in epithelial tissues. An important issue in this context was to determine whether the Goldman constant field equation approximates the experimentally determined data for the apical membrane over a reasonable range of values. This question is of importance for the following reasons.

(*a*) It has been shown that the *I-V* relation of the amiloride-sensitive pathway in other tight epithelia is fairly accurately described by the Goldman equation (Palmer et al., 1980; Frömter et al., 1981; Thompson et al., 1982*a*; Thomas et al., 1983). However, in the case of the frog skin, this has been disputed (Helman et al., 1979), which raises the question of whether the Goldman model represents a general property of tight epithelia.

(*b*) The permeability of the channels that are described by the Goldman equation is concentration- and voltage-independent. The curvature of the *I-V* relation of such a pathway is due solely to the asymmetry of ion concentration at the two openings of the channel (Lindemann, 1982). Thus, conformity with the Goldman equation eliminates at least certain possibilities for the permeation mechanism. For example, it is compatible neither with a single-file process (Hille and Schwarz, 1978) nor with a high density of fixed charges at the mouth of the channel (Lindemann, 1982). Moreover, models based on the Eyring rate theory for ion translocation can be used to make detailed speculations on pathway structures that are compatible with the Goldman equation and on the effects of modifying channel structure on the shape of the resulting *I-V* plot (Lindemann, 1982).

Our results show that when the cell current is plotted as a function of the apical membrane potential, the experimental points differ from those predicted by the Goldman equation by less than the experimental noise when time delays of ≤20 ms and potentials in the range between the transepithelial short-circuit point (V_{sc}) and the reversal potential (E_a) are examined. At more extreme potentials and at longer times, larger and relatively systematic deviations from

the theoretical curve were found. The close correspondence between the experimental and predicted points described here is similar to results obtained in a similar restricted range in other epithelia and justifies the suggestion that electrodiffusion should be the first mechanism to be considered in future studies analyzing the movement of Na^+ through the amiloride-sensitive channel. It is not clear whether the deviations at higher potentials and longer times indicate the presence of a totally different mechanism or are the consequence of relatively subtle differences in channel structure (for example, a nonuniform pattern of distribution of fixed charges, redistribution of charges with time and potential, etc.) from that required for a true Goldman rectification.

Evaluation of the Data

AMILORIDE ASSUMPTION We evaluated our data by equating the transcellular current with the amiloride-inhibitable current, in which the construction of the amiloride-inhibitable current vs. membrane voltage curves involves only the subtraction of pairs of experimentally determined quantities. The identification of the amiloride-inhibitable current with the cell current involves the following two assumptions.

(*a*) Amiloride does not affect the conductance of parallel pathways. Although there is substantial evidence that amiloride selectively inhibits the apical Na^+ channel of tight epithelia with little or no action on the ion movements through other pathways, there are some observations suggesting that amiloride affects, under certain circumstances, Cl^- movements across the skin (Candia, 1978; Kristensen, 1983). One of the observations most relevant to our study was reported by Kristensen (1983). He found that after the rapid addition of amiloride to the outside solution, there was a sudden drop in conductance that followed closely the time course of the depression in I_{sc}. This is, of course, what would be expected if amiloride blocks the apical membrane Na^+ conductance. However, subsequently there was a slow drop in conductance for the next ~2 min (see Fig. 9 of Kristensen, 1983). We also have seen such an effect; however, we would like to stress two features not mentioned by Kristensen (1983). First, in many skins immersed in Cl^- solutions, the slow change in conductance that followed the addition of amiloride was clearly observed only during the first addition of the diuretic. During subsequent additions, it was nearly undetectable or altogether absent. In practice, our measurements in Cl^- Ringer's were only performed when the slow effect could not be detected after the addition of amiloride. Second, we were able to avoid this problem entirely by performing experiments in a Cl^--free (SO_4^{2-}) Ringer's. In these solutions, the slow change in conductance was not observed. This observation supports Kristensen's proposal that we are dealing with a change in Cl^- conductance. More important for our purposes, it suggests that the distortions introduced into our results by any effect of amiloride on Cl^- conductance must be relatively small, since the basic behavior of the skin is similar in both Cl^- and SO_4^{2-} solutions.

(*b*) There is no leak pathway through the apical membrane in the presence of amiloride. This condition is almost completely met for our experiments, since we report here only results in which the fractional resistance of the apical

membrane in amiloride-treated skins ranged from 0.95 to 1.0 (Thompson et al., 1982*a*, *b*; Thomas et al., 1983).

THE TRANSIENT RESPONSES An interesting finding encountered early in this study was that the application of square voltage pulses leads to pronounced transient responses. Such transient behavior has been described before (e.g., Nagel, 1976; Weinstein et al., 1980). The existence of these transients gives rise to important methodological and theoretical problems. In particular, we would like to know how the transients affect the interpretation of the *I-V* data, i.e., when is the "correct" time to make the measurements, and what is the physical correlate of the transient within the tissue? Our measurements of the time course of the responses at the individual membranes lead to three interesting qualitative conclusions. First, the transients are probably due to the passage of current through the cellular pathway since they are eliminated by amiloride (cf. Fig. 3). Second, the transients appear to be generated mainly by the properties of the basolateral border: the *I-V* plot of the basolateral border was markedly modified by the time of sampling (cf. Figs. 11–13). In contrast, the behavior of the apical membrane was only mildly dependent on the time of sampling (Figs. 6–9). Major changes at this border were observed only when extreme transepithelial voltages were used. Third, when pulses up to several seconds long were used, the response could be described by the sum of two exponential terms (cf. Fig. 14).

In general, when measuring membrane conductance (and emf), measurements should be made as quickly as possible to avoid polarization effects that are due to the flow of ionic current through the membrane (the "transport number effect"; Barry and Hope, 1969). As we show below (*Kinetic Analysis of the Transient Responses*), there appears to be a large dielectric capacitance in the basolateral membrane. Hence, for the basolateral membrane, measurements at short times will not yield the true membrane conductance or emf, because it is necessary first to wait for this capacitance to charge. In addition, there does appear to be a transport number effect that partially overlaps in time with the effect of the dielectric capacitance. A further difficulty arises because the relative contribution of these two effects at different clamping potentials has not been determined. It thus appears that measurements at a single time do not provide a precise determination of g_b and E_b. In spite of these difficulties, we feel that measurements at 400 or 600 ms offer a meaningful approximation of basolateral parameters for the following reasons. (*a*) We expect that, at these times, the capacitance will be virtually completely charged, while the transport number effect, although significant, will still be relatively small. (*b*) The rate of change in the values calculated for g_b and E_b vs. time of sampling is slow in this time period (see Figs. 12 and 13). Hence, small variations in time constants between skins will not have a major effect on the interpretation of the *I-V* data.

The changes in V_a and V_b have the same time course because the apical and basal membranes are coupled through the voltage clamp. Therefore, strictly speaking, we should be able to use the same time for the apical membrane as for the basolateral membrane. On the other hand, the presence of polarization effects makes it, in principle, desirable to use as early a time to measure as possible. Since there does not appear to be a large dielectric capacitance at the

apical membrane, it should be possible to use such earlier times for the apical membrane. Accordingly, we have chosen to use 20 ms for analyzing the apical membrane parameters, although it appears that any time between ~2 and 40 ms would be suitable.

The Apical Barrier

Our results show that the *I-V* relation of the apical barrier of the frog skin is closely described by the Goldman constant field equation for a single ion over a range of potentials that extends over ~200 mV in skins incubated in a normal Cl^- or SO_4^{2-} Ringer's. The values of intracellular Na^+ activity calculated from our values of E_a (Table I), with the exception of our single *R. pipiens* when incubated in Cl^- solution, agree well with previous determinations of Na^+ in frog skin epithelium by other methods (Aceves and Erlij, 1971; Rick et al., 1978; Nagel et al., 1981). When the apical solution Na^+ concentration was lowered to one-fifth, the range of voltages over which agreement with the Goldman equation held was narrowed; however, the conformity was still quite satisfactory. Also, E_a was displaced, in relatively good agreement with the predictions of Eq. 4. In addition, we have found (Schoen and Erlij, 1983) that during the action of ouabain, the *I-V* relation still conforms closely to the Goldman equation, despite the fact that P_{Na} was depressed. In agreement with the well-known effects of ouabain, E_a was shifted as if cell Na^+ had increased. These findings, which show that the *I-V* relationship of the apical border conforms to the Goldman equation under a variety of circumstances, are consistent with the notion that Na^+ movements across the apical barrier occur by electrodiffusion through channels of relatively homogeneous properties.

The conformity of the *I-V* relation of the Na^+ pathway at the apical border to the Goldman equation is a property of the amiloride-sensitive channel of a variety of epithelia. This behavior has been observed in the *Necturus* urinary bladder (Frömter et al., 1981; Thomas et al., 1983) and rabbit colon (Thompson et al., 1982*a*). It is interesting that the conformity also holds in frog skins and toad urinary bladders in which transepithelial measurements were used after the contribution of the basolateral barrier was reduced by incubating the tissue with elevated $[K^+]$ in the serosal solution (Fuchs et al., 1977; Palmer et al., 1980). Therefore, it seems warranted to suggest that we are dealing with a general property of the amiloride-sensitive apical Na^+ channel. An important exception to this behavior has been reported by Helman et al. (1979). As we mentioned in the Introduction, these authors used a radically different approach to separate the current moving through transport and nontransport pathways in their microelectrode experiments. They based their distinction on the identification of E_{Na} with a particular value of the apical membrane potential, namely, $V_a = 0$. Evidently, this is the root of the discrepancy, since as shown by our results and those quoted above, when $V_a = 0$, there is still a substantial amiloride-sensitive current flow.

When the apical solution Na^+ concentration was lowered from 120 to 24 or 28 mM, the decline in E_a was 44.9 mV/decade, which is less than the 59 mV/

decade predicted by Eq. 4. This discrepancy could be due to a reduction in a^c_{Na} during the 1 min the skins were exposed to the reduced Na^+ concentration. Previous workers have suggested that reducing the apical Na^+ concentration in frog skin leads to a reduction in a^c_{Na} (Rick et al., 1978; Harvey and Kernan, 1984), although, in the experiments of Thomas et al. (1983) in *Necturus* urinary bladder, there was no need to propose that altering apical [Na^+] had any effect on a^c_{Na}. Assuming that our results are indeed due to a lowering of a^c_{Na}, we can use Eq. 4 to calculate a^c_{Na} from the value of E_a obtained for each skin. This calculation gives average values of 25.1 mM in control Ringer's and 17.2 mM in reduced [Na^+], and an average change of 7.9 mM (Table II). If we assume that the activity of the Na,K pump, and hence the rate of basolateral Na^+ efflux from the epithelium, are not altered by the reduction of apical [Na^+], then the reduction in I_{sc} resulting from reduced apical [Na^+] must be equivalent to the net rate of loss of Na^+ from the tissue. We can then calculate that the volume in which such a concentration change occurs corresponds to a layer 3.5 ± 1.5 μm deep. This is considerably less than the depth of the frog skin epithelium, and corresponds roughly to some estimates of the depth of the outermost living cell layer only (e.g., 2.6 μm; Martinez-Palomo et al., 1971).

As suggested by the electrical data in this study and in that of Smith (1971), as well as by the measurements of electrolyte concentrations in different cell layers of the skin by Rick et al. (1978), it appears that the cells of the frog skin are electrically coupled and changes in electrolyte concentration occur with some uniformity throughout all layers of the skin. On the other hand, there have been claims in the literature that only a portion of the epithelium is immediately involved in Na^+ transport. For example, Voûte and Ussing (1968) noted that only the outer layer of epithelial cells, which they called the "first reacting cell layer," swelled when the epithelium was short-circuited. Aceves and Erlij (1971) observed that only ~1/10 of the total Na^+ in the epithelium appeared to be labeled by Na^+ in the apical bath. Finally, Morel and Leblanc (1975) observed that, at least under the conditions of their experiments, alterations in the short-circuit current resulting from changes in apical solution [Na^+] occurred with a time constant of 0.5–1 min in actively transporting preparations, but with a longer time constant if transport was inhibited. They suggested that the changes in intracellular Na^+ levels are restricted to a small portion of the total epithelium in transporting skins and extend to the whole epithelium only if transport is inhibited.

An additional observation of our experiments was that, in agreement with previous studies (Fuchs et al., 1977), a reduction in the apical bath [Na^+] caused an increase in the apical membrane permeability to Na^+.

One additional point concerning the properties of the apical membrane emerges from our study. Fig. 15 shows g_a plotted against I_{sc} for each of the skins in Table I. This plot shows that I_{sc} is correlated with g_a. This relationship strongly suggests that the conductance of the apical membrane determines the rate of transepithelial transport. Indeed, similar relationships have been observed in other tight epithelia (e.g., Frömter and Gebler, 1977; Thomas et al., 1983).

Basolateral Membrane

The results reported here clearly show that most of the transient behavior in I_T and V_a is due to the properties of the basolateral membrane. The marked time dependence of the basolateral border *I-V* plots prevents us from obtaining a precise estimate of the parameters of the basolateral membrane from an analysis of the *I-V* relations alone. From our analysis of the transients (see THE TRANSIENT RESPONSES and the next section), we suggest that, for moderate transepithelial potentials, measurements made between 400 and 600 ms provide a reasonable approximation.

If the basolateral barrier has no conductance other than to K^+, then it should be possible to calculate a_K^c from E_b using the Nernst equilibrium equation. The overall average a_K^c calculated in this manner for each of the skins in Table I was

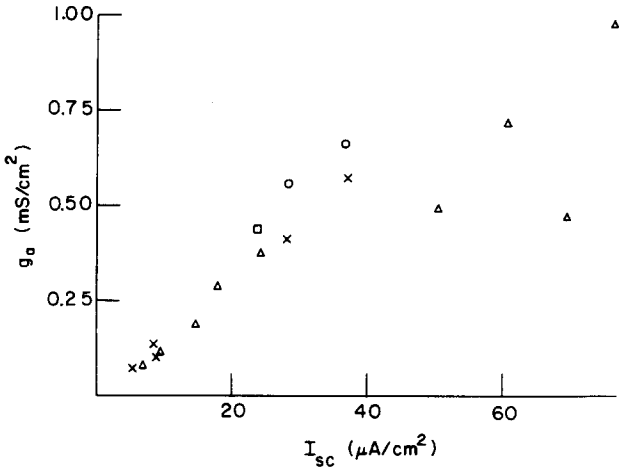

FIGURE 15. Plot of slope conductance (g_a) vs. I_{sc}. Each point represents an individual skin. △, *R. catesbeiana* in Cl^- Ringer's; ×, *R. catesbeiana* in SO_4^{2-} Ringer's; □, *R. pipiens* in Cl^- Ringer's; ○, *R. pipiens* in SO_4^{2-} Ringer's.

87.0 ± 15.8. This is lower than the values reported by most other authors. For example, Aceves and Erlij (1971) and Rick et al. (1978), using two different analytical techniques, reported values approximately equivalent to intracellular activities of 101 and 150 mM, respectively. Nagel et al. (1981), using K^+-selective electrodes, obtained an a_K^c of 132 mM, although Harvey and Kernan (1984), who also used K^+-selective electrodes, reported a lower activity of 70.3 mM. The presence of conductances to other ions in the basolateral membrane could contribute to the low values of E_b. A Cl^- conductance seems unlikely because the values of E_b were lower in sulfate solutions than in Cl^- solutions. A Na^+ conductance is, of course, another possibility. We have demonstrated that, at least under certain conditions, a significant permeability to Na^+ in the basolateral membrane can be induced (Schoen and Erlij, 1984). However, whether or not such a pathway is conductive is presently unknown.

Kinetic Analysis of the Transient Responses

In order to evaluate the *I-V* data in more detail, it was necessary to obtain more information about the nature of the transients. When experiments using pulses of several seconds' duration were performed, it was observed that the data appeared to be the sum of two exponential processes (Fig. 14) with time constants of 113.6 ± 20.0 and 1,563 ± 322 ms. Our development of the simplest circuit model that could explain this result proceeded as follows.

We first considered the circuit shown in Fig. 16*A*. The expressions describing

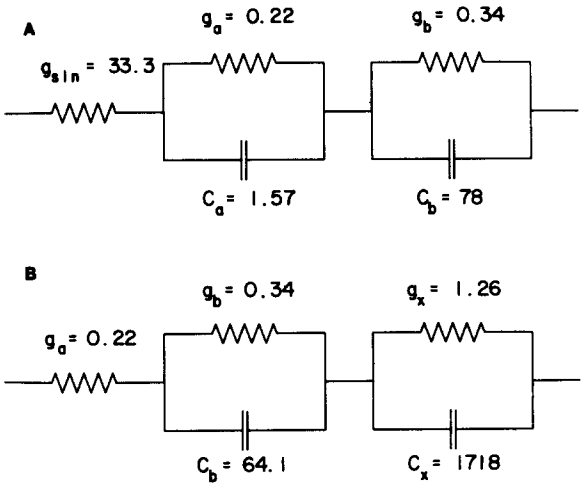

FIGURE 16. Electrical circuits used to model the transient responses of the skin (see text). Conductances are in millisiemens per square centimeter; capacitances are in microfarads per square centimeter.

the time constants of the current transient when a step voltage is applied to this circuit can be shown to be (see Appendix):

$$\tau_1 = \frac{2a}{b - (b^2 - 4ac)^{1/2}}; \tag{5a}$$

$$\tau_2 = \frac{2a}{b + (b^2 - 4ac)^{1/2}}, \tag{5b}$$

where

$$a = \frac{C_a C_b}{g_{sln} g_a g_b}; \tag{6a}$$

$$b = \frac{C_a}{g_a g_b} + \frac{C_b}{g_a g_b} + \frac{C_a}{g_{sln} g_a} + \frac{C_b}{g_{sln} g_b}; \tag{6b}$$

$$c = \frac{1}{g_a} + \frac{1}{g_b} + \frac{1}{g_{sln}}, \tag{6c}$$

as these terms are used in Fig. 16*A*. We evaluated this model by calculating the time constants that would result from the values of conductance measured for these three skins and a realistic value for capacitance. The values for g_a and g_b were measured essentially as described in Methods, i.e., using amiloride to allow the determination of I_m. The value of g_a was determined 20 ms after the beginning of the pulse, and the value of g_b was determined at ~400 ms. The interval used for determining g_b is long enough so that C_b should be almost completely charged. The presence of the additional conductance g_x (see below) should have a relatively minor contribution to the calculation of g_b at 400 ms. The solution conductance (g_{sln}) was chosen as 33.3 mS/cm^2.

For C_a and C_b, we used the values in Table II of Smith (1971), 1.57 and 78 μF/cm^2, respectively, determined by AC impedance locus analysis. As noted by Smith, these values are consistent with the total area of membrane material per unit area of skin (see below), assuming that the membrane capacitance is ~1 μF/cm^2.

The values for the electrical components discussed above are collected in Fig. 16*A*. The values of τ_1 and τ_2, calculated from these values using Eqs. 5 and 6, were 142 and 0.05 ms, respectively. Our measurements would miss a transient with a time constant of the order of τ_2, i.e., 0.05 ms, because they were not designed to detect very fast responses. The calculated value of τ_1 is similar to our measured time constant of 113.6 ms (τ_b, which corresponds to the open symbols in Fig. 14).

We also evaluated this model with a slightly different procedure. We let τ_1 equal our measured time constant of 113.6 ms and let τ_2 equal 0.05 ms. We then calculated a value for C_b using the same values as before for the other components of Fig. 16*A*. The value thus obtained for C_b was 68 μF/cm^2.

These calculations show that the presence of a time constant with the magnitude of τ_b can be explained by a circuit with components that have values similar to those proposed by Smith (1971). The fact that the *I-V* curves for only the basolateral border show large variations with time over the first few hundred milliseconds of the pulses (compare Figs. 6–9 with Figs. 11–13) adds further support to the proposal of Smith (1971), who identified the capacitance with the dielectric formed by all the membranes facing the basolateral solution and also suggested that all the cells are connected by low-resistance junctions.

The circuit developed thus far, however, does not completely describe our results since, as mentioned above, we found an additional exponential component with a time constant of 1,563 ms (τ_x, which corresponds to the lines drawn through the filled symbols in Fig. 14). To obtain an estimate of the additional passive electrical components that could generate such a time constant, we evaluated the model illustrated in Fig. 16*B*. Although the electrical circuit is the same as in Fig. 16*A*, the individual components correspond to different physical elements. g_x and C_x correspond to the additional components presumed to be responsible for the presence of an additional time constant.

The selection of this model requires some comment. We elected to represent the apical membrane by only a resistor for two reasons: (*a*) otherwise, the equation describing the circuit becomes unwieldy; (*b*) an evaluation of the circuit

shown in Fig. 16*A* showed that when $C_b \gg C_a$, the contribution of C_a to the value calculated for τ_1 is very small. For example, whereas the value calculated above for τ_1 with C_a taken as 1.57 μF/cm^2 was 142 ms, τ_1 with $C_a = 0$ would be 140 ms, i.e., virtually the same. We should also mention that the process responsible for the presence of an additional time constant is not known (see below), and therefore it is not clear whether it can be modeled as an RC circuit. Nevertheless, we decided to model it as an RC circuit, in agreement with the practice followed by previous workers (e.g., Noyes and Rehm, 1970).

The model in Fig. 16*B* was evaluated as follows. g_a and g_b were the same as used for the evaluation of Fig. 16*A*. g_x was evaluated from the relation $(1/g_x) = V_o/(I_m^{sc} - I_m^{inf}) - (1/g_a) - (1/g_b)$, where V_o is the size of the transepithelial voltage pulse. τ_1 and τ_2 in Eq. 5 were set equal to the experimentally determined values of τ_b and τ_x, and are described by Eq. 5, but now with:

$$a = \frac{C_b C_x}{g_a g_b g_x}; \tag{7a}$$

$$b = \frac{C_b}{g_b g_x} + \frac{C_x}{g_b g_x} + \frac{C_b}{g_a g_b} + \frac{C_x}{g_a g_x}; \tag{7b}$$

$$c = \frac{1}{g_a} + \frac{1}{g_b} + \frac{1}{g_x}. \tag{7c}$$

Eqs. 5 and 7 could then be solved for C_b and C_x. The resulting calculation gave a value for C_b of 64.1 ± 15.4 and for C_x of 1,718 ± 1,126 μF/cm^2. (Actually, when both capacitance values are unknown, there are two solution sets. The alternative solution set gave capacitance values of 690 ± 75 and 209 ± 158 μF/cm^2.)

It is satisfying that this calculation produces a value of C_b that is very close to that obtained with the model in Fig. 16*A*. The presence of g_x and C_x appears to have little influence on the value of τ_b and the calculated value of C_b. The large value calculated for C_x suggests that the physical counterpart of this component cannot be a dielectric capacitor. It is possible that it represents the development of concentration changes near the membrane(s) brought about by the flow of ionic current through the tissue ("transport number effect," Barry and Hope, 1969). A further study of the transient in the presence of agents that modify apical and basolateral membrane properties may provide additional clues to the origins of both of these components.

On the basis of the above interpretation of the transients, it seems that, to a first approximation, measurements between 400 and 600 ms are best for calculating the parameters of the basolateral membrane. However, we should point out that our kinetic analysis of the transient was done only at moderate transepithelial potentials. It is apparent from the *I-V* curve of the basolateral membrane (Fig. 11) that there is a dramatic decrease in the apparent membrane conductance at large hyperpolarizing potentials. This in turn could be expected to influence the time constants and make comparisons of one region of the *I-V* curve with another misleading.

APPENDIX

Derivation of Eq. 5

The impedance of a resistor in the frequency, or s, domain is $1/g$ and that of a capacitor is $1/sC$ (Nilsson, 1983, pp. 543–544), where s is the variable of the s domain. The impedance of the circuit in Fig. 16*A* can be written by combining the impedances of the individual components using the same rules of series and parallel combination that are used in the time domain. Hence, the total impedance of the circuit is

$$\begin{aligned} Z_{(s)} &= \frac{1}{g_{sln}} + \frac{1/(g_a sC_a)}{1/g_a + 1/sC_a} + \frac{1/(g_b sC_b)}{1/g_b + 1/sC_b} \\ &= \frac{1}{g_{sln}} + \frac{1}{g_a + sC_a} + \frac{1}{g_b + sC_b}, \end{aligned} \tag{A1}$$

where $Z_{(s)}$ is the impedance as a function of s. The emf's associated with the actual membrane barriers are ignored in this analysis because they are assumed to be the same before and after the voltage pulse is applied and therefore in theory do not contribute to the transient response.

When a voltage is applied across the circuit, the current response in the s domain is given by Ohm's law (Nilsson, 1983, pp. 500ff, 509ff, 543–544). Also, if the applied voltage is a voltage step V_o, then $V_{(s)} = V_o/s$. Hence,

$$I_{(s)} = \frac{V_{(s)}}{Z_{(s)}} = \frac{V_o}{sZ_{(s)}} = \frac{V_o}{s[1/g_{sln} + 1/(g_a + sC_a) + 1/(g_b + sC_b)]}, \tag{A2}$$

where $I_{(s)}$ and $V_{(s)}$ are, respectively, current and voltage as functions of s.

Rearranging Eq. A2 yields

$$I_{(s)} = \frac{V_o\left[s^2\left(\frac{C_aC_b}{g_ag_b}\right) + s\left(\frac{C_a}{g_a} + \frac{C_b}{g_b}\right) + 1\right]}{s\left[s^2\left(\frac{C_aC_b}{g_{sln}g_ag_b}\right) + s\left(\frac{C_a}{g_ag_b} + \frac{C_b}{g_ag_b} + \frac{C_a}{g_{sln}g_a} + \frac{C_b}{g_{sln}g_b}\right) + \left(\frac{1}{g_{sln}} + \frac{1}{g_a} + \frac{1}{g_b}\right)\right]}. \tag{A3}$$

Eq. A3 can be simplified by applying the equalities of Eq. 6 to the expressions within the parentheses in its denominator. In addition, we add two more equalities for the values in parentheses in the numerator:

$$d = \frac{C_aC_b}{g_ag_b}; \tag{A4a}$$

$$e = \frac{C_a}{g_a} + \frac{C_b}{g_b}. \tag{A4b}$$

Substituting all these equalities into Eq. A3 gives

$$I_{(s)} = \frac{V_o(ds^2 + es + 1)}{s(as^2 + bs + c)}. \tag{A5}$$

We let s_1 and s_2 equal the roots of the quadratic expression in the denominator of Eq. A5, viz.,

$$s_1 = \frac{-b + (b^2 - 4ac)^{1/2}}{2a}; \tag{A6a}$$

$$s_2 = \frac{-b - (b^2 - 4ac)^{1/2}}{2a}. \tag{A6b}$$

Partial fraction expansion of Eq. A5 (Nilsson, 1983, pp. 518ff) then yields:

$$I_{(s)} = V_o\left[\frac{1}{c}\cdot\frac{1}{s} + \frac{ds_1^2 + es_1 + 1}{as_1(s_1 - s_2)}\cdot\frac{1}{s - s_1} + \frac{ds_2^2 + es_2 + 1}{as_2(s_2 - s_1)}\cdot\frac{1}{s - s_2}\right]. \tag{A7}$$

Taking the inverse Laplace transform:

$$I_{(t)} = V_o\left[\frac{1}{c} + \frac{ds_1^2 + es_1 + 1}{as_1(s_1 - s_2)}\,e^{-u_1} + \frac{ds_2^2 + es_2 + 1}{as_2(s_2 - s_1)}\,e^{-u_2}\right], \tag{A8}$$

where t is time and $I_{(t)}$ is the current as a function of t.

The time constants from Eq. A8 are therefore

$$\tau_1 = \frac{1}{-s_1} = \frac{2a}{b - (b^2 - 4ac)^{1/2}}; \tag{A9a}$$

$$\tau_2 = \frac{1}{-s_2} = \frac{2a}{b + (b^2 - 4ac)^{1/2}}. \tag{A9b}$$

We thank Dr. Sandy Helman for providing assistance in the building of the voltage clamp and the microelectrode amplifier used in our early experiments. We also thank Dr. Steve Fox for his help in deriving the equations for the time constants.

This project was supported by grants 24064 and 33612 from the Arthritis and Metabolic Diseases Institute, Department of Health and Human Services, and by a grant-in-aid from the New York Heart Association.

Original version received 14 November 1983 and accepted version received 5 April 1985.

REFERENCES

Aceves, J., and D. Erlij. 1971. Sodium transport across the isolated epithelium of the frog skin. *J. Physiol. (Lond.).* 212:195–210.

Barry, P. H., and A. B. Hope. 1969. Electroosmosis in membranes: effects of unstirred layers and transport numbers. I. Theory. *Biophys. J.* 9:700–728.

Candia, O. A. 1978. Reduction of chloride fluxes by amiloride across the short-circuited frog skin. *Am. J. Physiol.* 234:F437–F445.

Dixon, W. J., editor. 1983. BMDP Statistical Software. University of California Press, Berkeley, CA. 290–304.

Frömter, E., and B. Gebler. 1977. Electrical properties of amphibian urinary bladder epithelia. III. The cell membrane resistances and the effect of amiloride. *Pflügers Arch. Eur. J. Physiol.* 371:99–108.

Frömter, E., J. T. Higgins, and B. Gebler. 1981. Electrical properties of amphibian urinary bladder epithelia. IV. The current voltage relationships of the sodium channels in the apical cell membrane. *In* Ion Transport in Epithelia. S. G. Schultz, editor. Raven Press, New York. 31–45.

Fuchs, W., E. H. Larsen, and B. Lindemann. 1977. Current-voltage curve of sodium channels and concentration dependence of sodium permeability in frog skin. *J. Physiol. (Lond.).* 267:137–166.

Goldman, D. E. 1943. Potential, impedance, and rectification in membranes. *J. Gen. Physiol.* 27:37–60.

Harvey, B. J., and R. P. Kernan. 1984. Intracellular ion activities in frog skin in relation to external sodium and effects of amiloride and/or ouabain. *J. Physiol. (Lond.).* 349:501–517.

Helman, S. I., and R. S. Fisher. 1977. Microelectrode studies of the active Na transport pathway of frog skin. *J. Gen. Physiol.* 69:571–604.

Helman, S. I., and D. A. Miller. 1971. In vitro techniques for avoiding edge damage in studies of frog skin. *Science (Wash. DC)*. 173:146–148.

Helman, S. I., W. Nagel, and R. S. Fisher. 1979. Ouabain on active transepithelial sodium transport in frog skin. *J. Gen. Physiol.* 74:105–127.

Helman, S. I., R. G. O'Neil, and R. S. Fisher. 1975. Determination of the E_{Na} of frog skin from studies of its current-voltage relationship. *Am. J. Physiol.* 229:947–951.

Hille, B., and W. Schwarz. 1978. Potassium channels as multi-ion single-file pores. *J. Gen. Physiol.* 72:409–442.

Hodgkin, A. L., and P. Horowicz. 1959. The influence of potassium and chloride ions on the membrane potential of single muscle fibres. *J. Physiol. (Lond.)*. 148:127–160.

Hodgkin, A. L., and B. Katz. 1949. The effect of sodium ions on the electrical activity of the giant axon of the squid. *J. Physiol. (Lond.)*. 108:37–77.

Kristensen, P. 1983. Exchange diffusion, electrodiffusion and rectification in the chloride transport pathway of frog skin. *J. Membr. Biol.* 72:141–151.

Lindemann, B. 1982. Dependence of ion flow through channels on the density of fixed charges at the channel opening. Voltage control of inverse titration curves. *Biophys. J.* 39:15–22.

Martinez-Palomo, A., D. Erlij, and H. Bracho. 1971. Localization of permeability barriers in the frog skin epithelium. *J. Cell Biol.* 50:277–287.

Morel, F., and G. Leblanc. 1975. Transient current changes and Na compartmentalization in frog skin epithelium. *Pflügers Arch. Eur. J. Physiol.* 358:135–157.

Nagel, W. 1976. The intracellular electrical potential profile of the frog skin epithelium. *Pflügers Arch. Eur. J. Physiol.* 365:135–143.

Nagel, W., J. F. Garcia-Diaz, and W. McD. Armstrong. 1981. Intracellular ionic activities in frog skin. *J. Membr. Biol.* 61:127–134.

Nilsson, J. W. 1983. Electric Circuits. Addison-Wesley, Reading, MA. 789 pp.

Noyes, D. H., and W. S. Rehm. 1970. Voltage response of frog gastric mucosa to direct current. *Am. J. Physiol.* 219:184–192.

Palmer, L. G., I. S. Edelman, and B. Lindemann. 1980. Current-voltage analysis of apical sodium transport in toad urinary bladder: effects of inhibitors of transport and metabolism. *J. Membr. Biol.* 57:59–71.

Rick, R., A. Dorge, E. V. Arnim, and K. Thurau. 1978. Electron microprobe analysis of frog skin epithelium: evidence for a syncytial sodium transport compartment. *J. Membr. Biol.* 39:313–331.

Robinson, R. A., and R. H. Stokes. 1965. Electrolyte Solutions. Second revised edition. Butterworths, London. 229–233.

Schoen, H. F., and D. Erlij. 1981*a*. Sodium current across apical border of frog skin is described by the Goldman constant field equation. *Physiologist.* 24:56. (Abstr.)

Schoen, H. F., and D. Erlij. 1981*b*. EMF across cell membranes of frog skin. Seventh International Biophysics Congress, Mexico City. 349. (Abstr.)

Schoen, H. F., and D. Erlij. 1982. Transient responses and electrodiffusion across apical barrier of frog skin. *Fed. Proc.* 41:1263. (Abstr.)

Schoen, H. F., and D. Erlij. 1983. Effects of ouabain on the apical and basolateral membranes of frog skin. *Fed. Proc.* 42:1101. (Abstr.)

Schoen, H. F., and D. Erlij. 1984. Outward sodium fluxes across the cellular pathway in tight epithelia. *Biophys. J.* 45:138*a*. (Abstr.)

Smith, P. G. 1971. The low-frequency electrical impedance of the isolated frog skin. *Acta Physiol. Scand.* 81:355–366.

Thomas, S. R., Y. Suzuki, S. M. Thompson, and S. G. Schultz. 1983. Electrophysiology of *Necturus* urinary bladder. I. "Instantaneous" current-voltage relations in the presence of varying mucosal sodium concentrations. *J. Membr. Biol.* 73:157–175.

Thompson. S. M., Y. Suzuki, and S. G. Schultz. 1982*a*. The electrophysiology of rabbit descending colon. I. Instantaneous transepithelial current-voltage relations and the current-voltage relations of the Na-entry mechanism. *J. Membr. Biol.* 66:41–54.

Thompson, S. M., Y. Suzuki, and S. G. Schultz. 1982*b*. The electrophysiology of rabbit descending colon. II. Current-voltage relations of the apical membrane, the basolateral membrane, and the parallel pathways. *J. Membr. Biol.* 66:55–61.

Van Driessche, W., and B. Lindemann. 1979. Concentration dependence of currents through single sodium-selective pores in frog skin. *Nature (Lond.)*. 282:519–520.

Voûte, C. L., and H. H. Ussing. 1968. Some morphological aspects of active sodium transport. The epithelium of the frog skin. *J. Cell Biol.* 36:625–638.

Weinstein, F. C., J. J. Rosowski, K. Peterson, Z. Delalic, and M. M. Civan. 1980. Relationship of transient electrical properties to active sodium transport by toad urinary bladder. *J. Membr. Biol.* 52:25–35.

Wills, N. K., D. C. Eaton, S. A. Lewis, and M. S. Ifshin. 1979. Current-voltage relationship of the basolateral membrane of a tight epithelium. *Biochim. Biophys. Acta.* 555:519–523.